SELF-HEALING CAPACITY OF CEMENTITIOUS COMPOSITES: EXPERIMENTS AND MODELING

Liberato Ferrara[a]**, Antonio Caggiano**[b]**, Visar Krelani**[a] **and Guillermo Etse**[b]

[a]*Politecnico di Milano, Milan, Italy. E-mails: liberato.ferrara@polimi.it, visar.krelani@polimi.it.*

[b]*CONICET and Universities of Buenos Aires and Tucuman, Argentina. E-mails: acaggiano@fi.uba.ar, getse@herrera.unt.edu.ar.*

Keywords: Self-healing, cementitious composites, zero-thickness interfaces, fracture mechanics, porosity.

Abstract. This paper aims at a thorough characterization of the self-healing capacity of cementitious composites, i.e. their capacity to completely or partially re-seal cracks and, in case, also exhibit recovery of mechanical properties. This problem will be investigated through both experiments and modeling with reference of a normal strength concrete under different types of exposure: i.e., air exposure and water immersion. The effects of the self-healing phenomena on the recovery of stiffness and load-bearing capacity have been evaluated by means of 3-point bending tests performed up to controlled crack opening and up to failure, respectively before and after conditioning. With reference to the modeling issue, an interface fracture based model, formulated and calibrated by the second and fourth author for the description of fracture processes in concrete, has been herein extended to include the effects of crack healing, through suitably defined functions which affect the time evolution of mechanical properties of concrete. Sensitivity to the effects of different parameters, e.g. tensile strength, fracture energy etc. will also be discussed. The obtained promising results stand as the first step for the development of a comprehensive "durability based" framework through which the effects of crack healing in cementitious composites could be consistently included into predictive modeling and design of concrete structures. Both the experimental analysis and the theoretical formulation proposed in this work stem out from the European Project "EnCoRe" (FP7-PEOPLE-2011-IRSES n. 295283; www.encore-fp7.unisa.it) funded by the European Union as part of the Seventh Framework Programme.

1 INTRODUCTION

Worldwide increasing consciousness for sustainable use of natural resources has made a challenging task the apparently contradictory requirements of using low cost materials and at the same time with high performance, in the field of Structural Engineering. The importance of sustainability as a requisite which has to inform structure concept and design has been also recently highlighted in the new Model-Code (2010). In this context, the availability of self-healing technologies, by controlling and repairing early-stage cracks in concrete structures, where possible, could, on the one hand, prevent permeation of driving factors for deterioration, thus extending the structure service life, and, on the other hand, even provide partial recovery of relevant engineering properties of the material (Van Tittelboom and De Belie, 2013; Wu et al., 2012).

Discovered as early as in 1836 by the French Academy of Science, and attributed to the transformation of calcium hydroxide ($Ca(OH)_2$) into calcium carbonate ($CaCO_3$) as a consequence of exposure to the carbon dioxide (CO_2) in the atmosphere, plenty of researchers demonstrated that concrete, under favourable conditions, can heal naturally without any particular additive (Hearn and Morley, 1997; Reinhardt and Jooss, 2003; Yang et al., 2009). This phenomenon known in literature as "autogenous healing" is the consequence of two main reactions (Neville, 2002): the first one deals with the reaction of unhydrated particles due to possible water ingress into cracks (Granger et al., 2007) while the second one is due to the precipitation of calcium carbonate as consequence of the reaction between calcium, contained in the cementitious matrix, with carbon dioxide dissolved in the water (Edvardsen, 1999).

Consensus among the international community has been achieved about the engineering significance of the problem, which has resulted in State-of-the-Art reports to be compiled as well as into a clear terminology definition. The RILEM TC-221-SHC "Self-healing phenomena in cement based materials" (Mihashi and Nishiwaki, 2012), distinguishes: (i) "self-closing" between and "self-healing": the first terms deals with the only closure of the cracks while the second phenomenon regards the restoring of the mechanical properties; (ii) based on the process of the action, between "autogenic" (or natural) and "autonomic" (or engineered) self-closing/healing, whether the crack closure or restoration of material properties is due to either the concrete material itself or some engineered addition.

In the very last decade a huge amount of research work has been dedicated to "engineered" self-healing, along different main directions of investigation. Particularly, the use of the so-called "crystalline additives" has been successfully explored (Sisomphon et al., 2012). These additive contain substances which react with cement constituents and form calcium silicate hydrates and have been already employed for the reduction of concrete porosity and of water permeability of concrete: as a matter of fact it can also effectively employed as self-healing engineering additions (Ferrara et al., 2014).

Only few models were developed in scientific literature to describe the self-healing phenomenon in cementitious composites. Some models were proposed to determine the amount of unhydrated cement particles in concrete specimens considering as input parameters the water-to-cement ratio and cement fineness (He et al., 2011, 2009). Recently, a model aimed at simulating further hydration using water transport theory, ion diffusion theory and thermodynamics theory was proposed by Huang and Ye (2012). However, these models do not provide any information about the mechanical effects of self-healing. Then, a hydro-chemo-mechanical model was developed by Hilloulin et al. (2014) to simulate the autogenous healing by further hydration with the aim to explain the mechanical regains after healing.

Recently, Di Luzio et al. (2014) provided a modeling approach, based on the Solidification-Microprestress-Microplane (SMM) model by Di Luzio and Cusatis (2013), which makes use of the microplane model $M4$ and the solidification micro-prestress theory and have incorporated in it self healing effect through a suitably defined internal variable, which accounts for the effects of cracking on diffusivity and the opposite recovering effect due to crack healing.

In this paper an experimental methodology is proposed to evaluate the effects of crack healing on the mechanical properties of concrete, with reference to both autogenic self-healing and engineered through the addition of a crystalline admixture. The crystalline admixture employed in this study, which will be described in the forthcoming section, consists of a mix of cement, sand and active silica and is added to the raw concrete constituents before mixing. The proposed methodology, which will also be described in detail in the forthcoming section, is based on 3-point bending tests performed up to controlled crack opening and up to failure, respectively before and after exposure/conditioning. With reference to this latter issue both immersion in water and exposure to open air have been considered, up to one year. The effects of the self-healing of cracks on the recovery of stiffness and load-bearing capacity have been evaluated. The results thus garnered were instrumental in defining and quantifying self-healing related indices, which could be implemented into a durability based design framework, as currently addressed by international design codes. Beside the experimental study, an interface fracture based model has been proposed to include the effects of crack healing, through suitably defined porosity-based functions which affect the time evolution of mechanical properties of concrete.

After this introduction, Section 2 describes the main results of the proposed experimental results. Then, Section 3 highlights the formulation of the proposed porosity-based interface model for simulating the observed cracking and post-cracking behaviour of the considered 3-point bending beams. Comparisons between experimental data and numerical predictions are presented and discussed in Section 4, then, Section 5 remarks the key results of the present research and figures out its possible future steps.

2 EXPERIMENTAL CAMPAIGN

2.1 Experimental methodology

The mix composition of the normal strength concrete employed in this study is detailed in Table 1. Because of the interest to evaluate the effects of crystalline additives on the self-healing capacity of concrete, a companion mix has been also produced with a 1% additive addition, by weight of cement. The additive was dry mixed with the raw aggregates, at the very beginning of the mixing sequence, which was then followed by addition of cement and, upon further mixing, by the incorporation of water and superplasticizer. The particles of the employed crystalline admixture are shown in Figure 1. They have irregular shape and size in the range of about $1-20\ \mu m$; their morphology is similar to that of cement grains. The EDS microanalysis in Figure 2 highlights the presence of calcium, oxygen, silicon, magnesium, aluminium and potassium. This spectrum is comparable with that of an Ordinary Portland Cement (OPC), except for the peak of sulphur which is slightly higher.

Concrete slabs with $1\ m$ long $\times\ 0.5\ m$ wide and $50\ mm$ thick were casted with and without the additive; after three days curing in fog room at $20\ ^oC$ temperature, 95% Relative Humidity (RH) and under wet towels, they were cut into prismatic "beam-like" specimens each $500\ mm$ long and about $100\ mm$ wide. Specimens were cured in the same fog room, for a period ranging between 35 and 42 days. Along the curing period the development of strength was monitored, for both concrete mixes, by means of compressive strength tests on $150\ mm^3$ cube companion

Table 1: Mix composition of investigated concretes (dosages in kg/m^3).

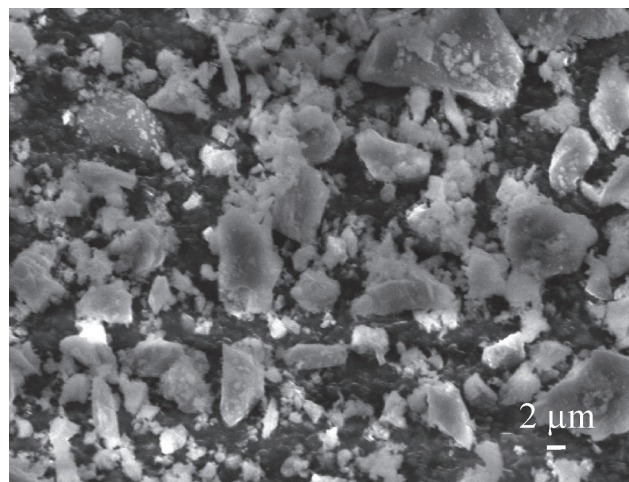| Constituent	Without additive	With additive
Cement type II 42.5	300	300
Water	190	190
Superplasticizer (lt/m^3)	3	3
Fine aggregate 0-4 mm	1078	1080
Coarse aggregate 4-16 mm	880	880
Crystalline additive	=	3

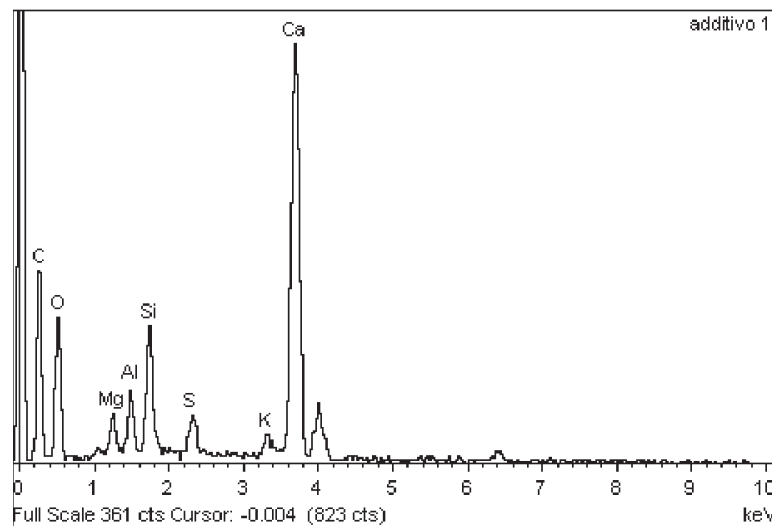Figure 1: SEM images of a powder sample of crystalline particles.

Figure 2: EDS analysis of the additive crystalline particles.

specimens. Results plotted in Figure 3 clearly show that the addition of crystalline admixtures had scant effect on the strength development.

In order to evaluate the self-healing capacity of concrete and its effects on the recovery of mechanical properties, at the end of the aforementioned curing period, the beam specimens were pre-cracked, up to different levels of residual crack opening, equal to about 100 and 200
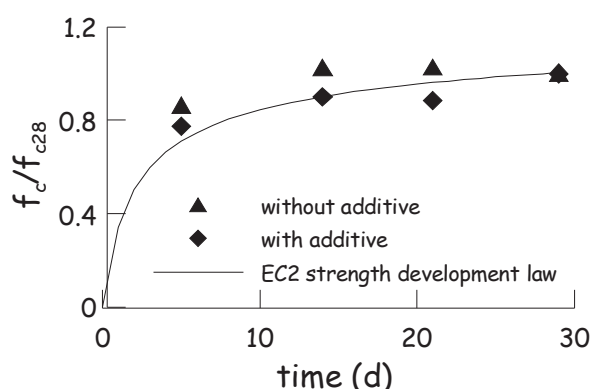
Figure 3: Strength development of concrete with and without crystalline additives in front of the EC2 provisions ($f_{c28} = 29.9\ MPa$ and $27.4\ MPa$ for concrete without and with the crystalline additive respectively: each data point represents the average value of two nominally identical tests).
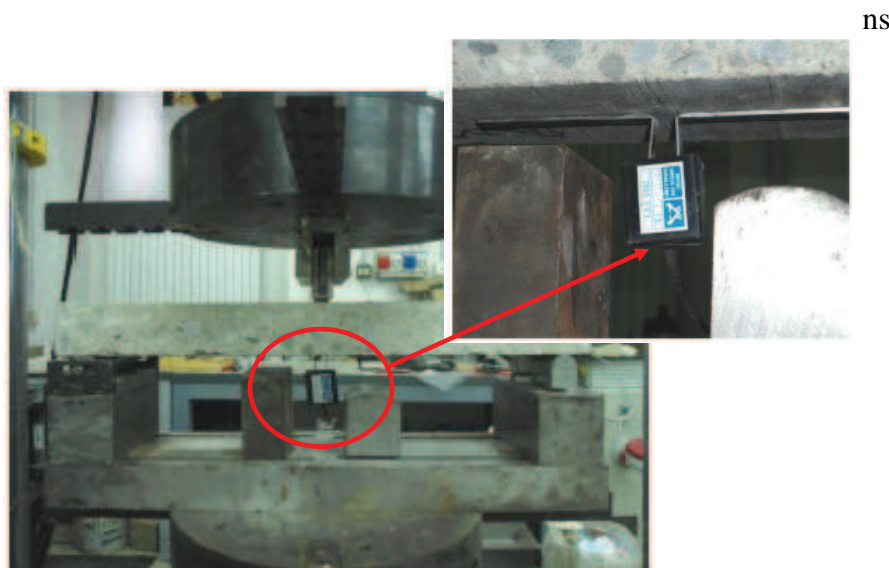

Figure 4: 3-point bending test set-up for specimen pre-cracking (beam span $= 450\ mm$).

μm. Particularly, such a specimens were pre-cracked employing the three-point bending (3pb) test set-up shown in Figure 4: the tests were performed using a clip gauge measuring the Crack Opening Displacement (COD) at mid-span, being COD the control variable. Some specimens were kept un-cracked for reference as well. All the specimens were then subjected to different controlled exposure conditions:

- immersion in water at constant temperature equal to $20\ ^oC$, up to 1 year;

- exposure to air, up to 1 year, while daily recording minimum and maximum temperature with the average RH, whose trends are plotted in Figure 5.

At the end of the scheduled exposure times, the 3pb tests were again performed on all specimens up to the complete failure (it is worth remarking that all specimens were, in case, wiped and allowed for a couple of hours to reach the condition of stable $20\ ^oC$ and $65\ \%$ RH, before the final tests). The nominal bending stress vs. COD response exhibited by the same specimen in its virgin state, i.e. when undergoing the pre-cracking stage test, and at the end of the prescribed exposure condition and duration in the cracked state were compared. The recovery, if
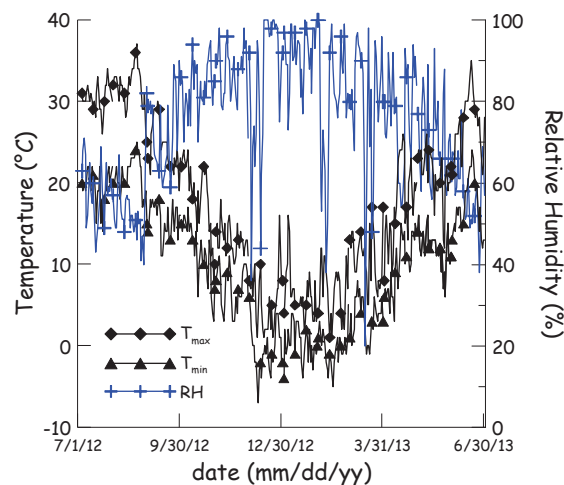
Figure 5: Temperature and Relative Humidity recorded along the exposure period.

any, of stiffness and load bearing capacity, as attributable to crack healing phenomena, will be thus evaluated, as it will be detailed in the forthcoming section. The obtained results were used at defining and quantifying suitable self-healing indices for the analyzed mechanical properties.

2.2 Experimental results: analysis and discussion

The results of a typical test 3-point bending tests are shown in Figure 6a, in terms of nominal stress σ_N vs. COD curves. It is worth remarking that the graphs are built up in such a way that the curves, pertaining respectively to the pre-cracking test and to the post-conditioning failure test, can be compared. Data were analyzed in order to define and calculate the self-healing Index of Load Recovery (ILR), defined as:

$$ILR = \frac{\sigma_{\text{N,maxreloading,post}-\text{conditioning}} - \sigma_{\text{unloading,pre}-\text{crack}}}{f_{ctf} - \sigma_{\text{unloading,pre}-\text{crack}}}. \tag{1}$$
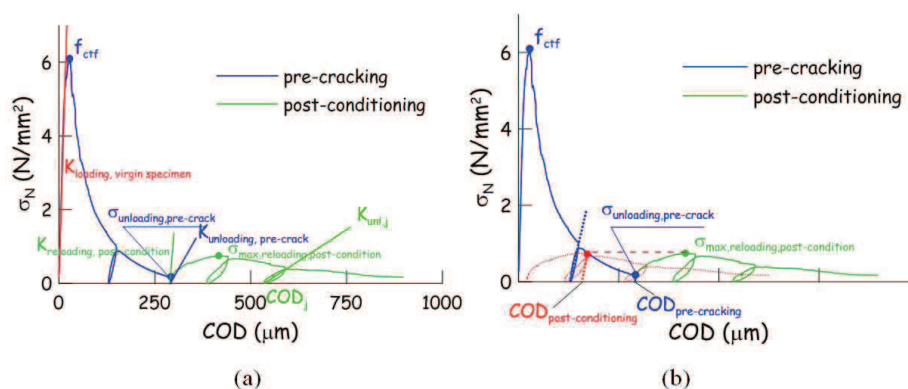

Figure 6: Example of stress vs. COD curves for specimens submitted to pre-cracking and post-conditioning 3pb tests: a) definition of quantities for calculation of self healing indices and b) graphical explanation of the procedure to estimate crack closure from σ_N-COD curves.

Figure 7 shows the trend of the ILR, computed as above, vs. the exposure time. Based on the results highlighted in Figure 7, it can be itemized the following remarks:

- Specimens immersed in water showed, since from the beginning, some load recovery capacity, which was higher for specimens containing the crystalline additive, and continued
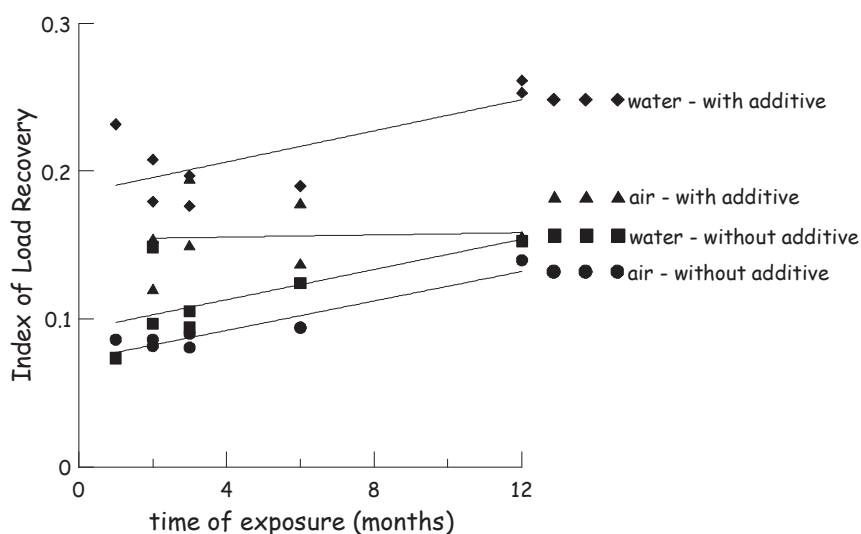
Figure 7: Index of Load Recovery vs. exposure time for water immersion/air exposure.
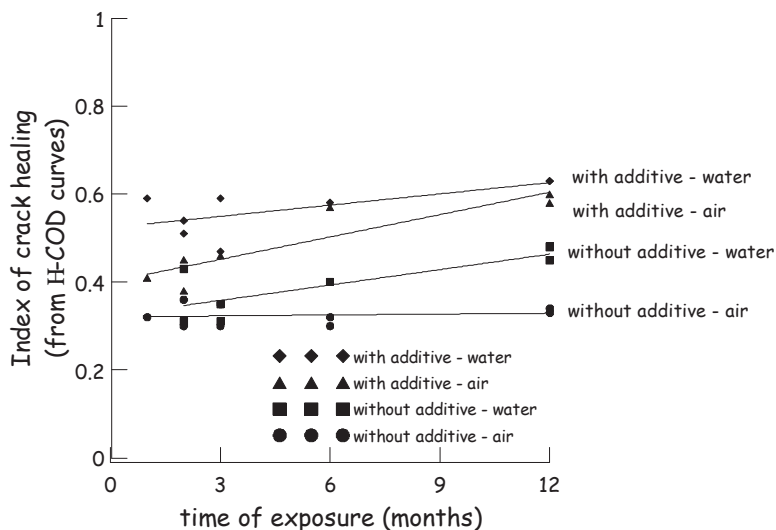

Figure 8: Index of Crack Healing vs. exposure time for water immersion/air exposure.

to moderately increase with immersion time, with similar trend for specimens with and without the additive; the maximum attained level of load recovery was not higher than 25% of the softening stress decay experienced upon pre-cracking;

- specimens exposed to air and containing the additive showed an initial load recovery capacity lower than specimens with the additive immersed in water but higher than all specimens without the additive; this confirms that additive particles, because of their hydrophilic nature, can capture air moisture and react with it promoting self-healing; nonetheless, the recovery did not exhibit significant changes upon prolonged exposure, as a combined effect of the consumption of the available crystalline additive and of the moisture available in the air, as also affected by daily and seasonal fluctuations;

- specimens exposed to air and without the crystalline additive showed, as expected, the lowest performance in terms of load recovery capacity due to self-healing, even with a moderately increasing trend, as resulting from the available air moisture and the kinetic

of delayed hydration of un-hydrated cement particles exposed upon cracking.

Moreover, from the nominal bending stress σ_N vs. COD curves as well as from the damage vs. COD evolution laws, an estimation of the crack closure due to the self-healing can be provided.
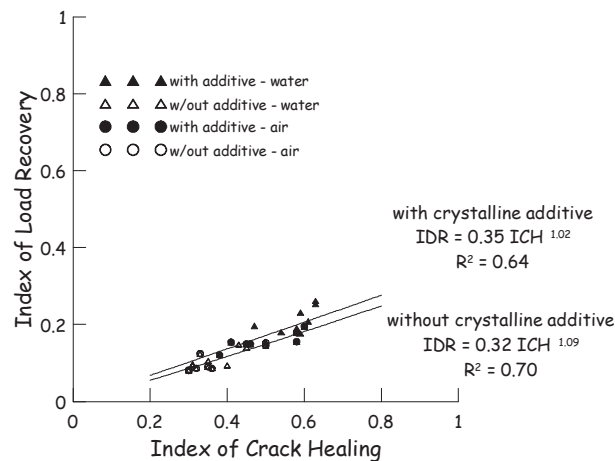

Figure 9: Index of Load Recovery vs. Index of Crack Healing as evaluated from stress vs. COD curves obtained from 3pb tests.
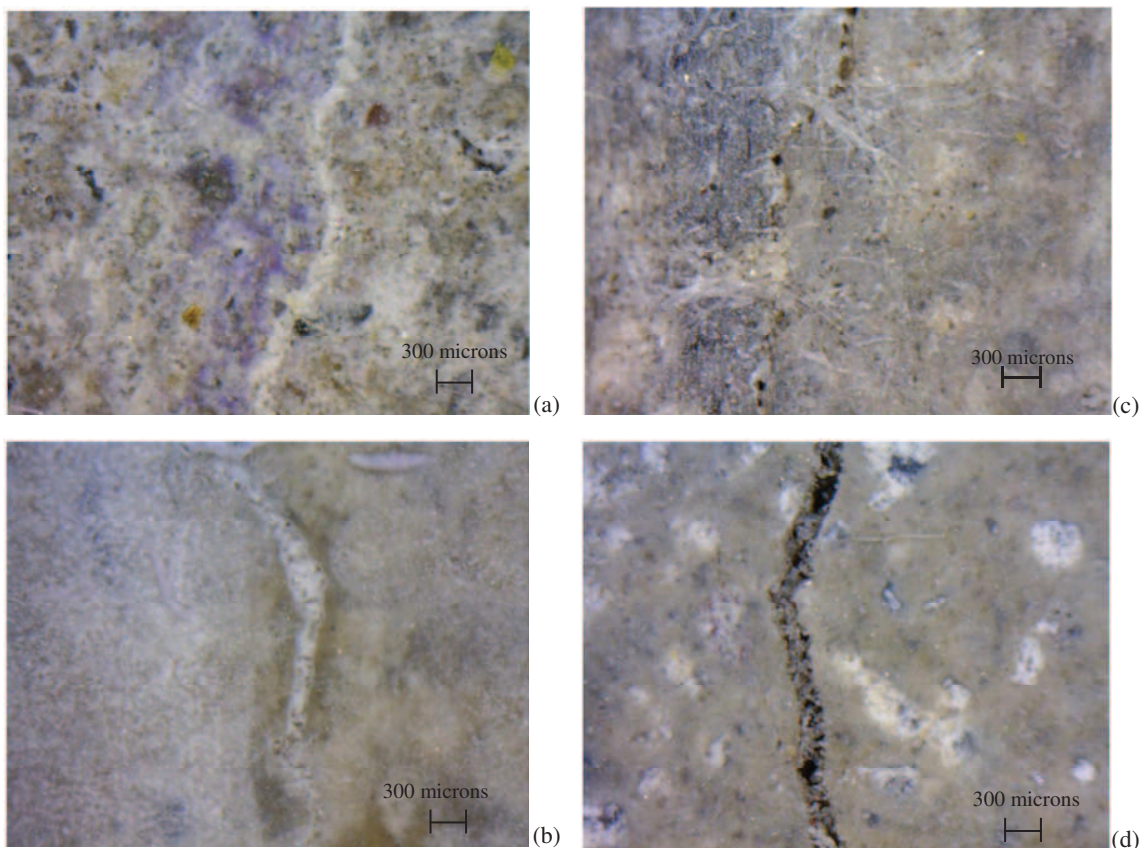

Figure 10: Healing cracks for specimens with (a) and without (b) crystalline additive after six months of immersion in water; with (c) and without (d) crystalline additive after six months of exposure to open air.

Following the procedure proposed in Ferrara et al. (2014), the index of crack healing, similar to that proposed in Eq. (1), has been proposed as

$$ICH_{\text{stress-crackopening}} = \frac{COD_{pre-cracking} - COD_{post-conditioning}}{COD_{pre-cracking}}. \tag{2}$$

The proposed methodology (graphically outlined in Figure 6b) consists in operating a "backward" shifting, along the COD axis, of the stress-COD curve representative of the behavior of each pre-cracked specimen after environment conditioning, until the stress-COD curve of the same specimen, as measured during the pre-cracking test on the virgin undamaged sample is met. The new value of the "origin" COD can be estimated by drawing, from the aforementioned point on the curve of the virgin sample, an unloading branch with a slope equal to that of the closest unloading previously measured on the virgin sample itself.

Figure 8 reports the measured index of crack healing vs. exposure time for both water immersion and air exposure. Then, the trend of the load recovery vs. crack healing (reported in Figure 9) demonstrated that some load bearing capacity is recovered even for very low values of estimated crack healing, with a more moderate influence of the additive, also considering the narrow data range provided by experiments. The captured trend is slower than the stiffness recover and hardly more than 20% of the stress decay experienced upon cracking could be garnered because of the crack healing. A better understanding could be achieved through a dedicated analysis of the strength development of crack healing products, as also affected by exposure conditions, which has been regarded as out of the scope of this work. Pictures obtained by stereo-microscope in Figures 10 confirm the related findings.

3 PORO-PLASTICITY FRACTURE-BASED INTERFACE MODEL

This section summarises the porosity dependent interface model for inelastic behaviour of joints of quasi-brittle materials like concrete. The model, based on a modification of the original proposal by Carol et al. (1997), is characterised by the following constitutive equations in rate form

$$\begin{aligned}
\dot{\mathbf{u}} &= \dot{\mathbf{u}}^{el} + \dot{\mathbf{u}}^{cr} \\
\dot{\mathbf{u}}^{el} &= \mathbf{C}^{-1} \cdot \dot{\mathbf{t}} \\
\dot{\mathbf{t}} &= \mathbf{C} \cdot (\dot{\mathbf{u}} - \dot{\mathbf{u}}^{cr})
\end{aligned} \tag{3}$$

where $\dot{\mathbf{u}} = [\dot{u}, \dot{v}]^t$ is the rate of the relative joint displacement vector, decomposed into the elastic and plastic components, $\dot{\mathbf{u}}^{el}$ and $\dot{\mathbf{u}}^{cr}$, respectively. C defines the normal/tangential elastic stiffness matrix,

$$\mathbf{C} = \begin{pmatrix} k_N & 0 \\ 0 & k_T \end{pmatrix} \tag{4}$$

while $\dot{\boldsymbol{t}} = [\dot{\sigma}_N, \dot{\sigma}_T]^t$ is the incremental stress vector defined in the interface coordinates, being σ_N and σ_T the normal and shear components, respectively.

The vector of the plastic displacement rate, according to the non-associated flow rule, is defined as

$$\dot{\mathbf{u}}^{cr} = \dot{\lambda}\mathbf{m} \tag{5}$$

where $\dot{\lambda}$ is the non-negative plastic multiplier which follows from the classical Kuhn-Tucker loading/unloading and consistency conditions

$$\begin{aligned}
\dot{\lambda} &\geq 0, \quad f \leq 0, \quad \dot{\lambda}f = 0 \quad &\text{Kuhn} - \text{Tucker} \\
\dot{f} &= 0 &\text{Consistency}
\end{aligned} \tag{6}$$

being $f = f[\sigma_N, \sigma_T]$ the yield condition of the model defined by means of the following three-parameter criterion (outlining the hyperbola represented in Figure 11)

$$f = \sigma_T^2 - (c - \sigma_N \tan\phi)^2 + (c - \chi \tan\phi)^2. \tag{7}$$

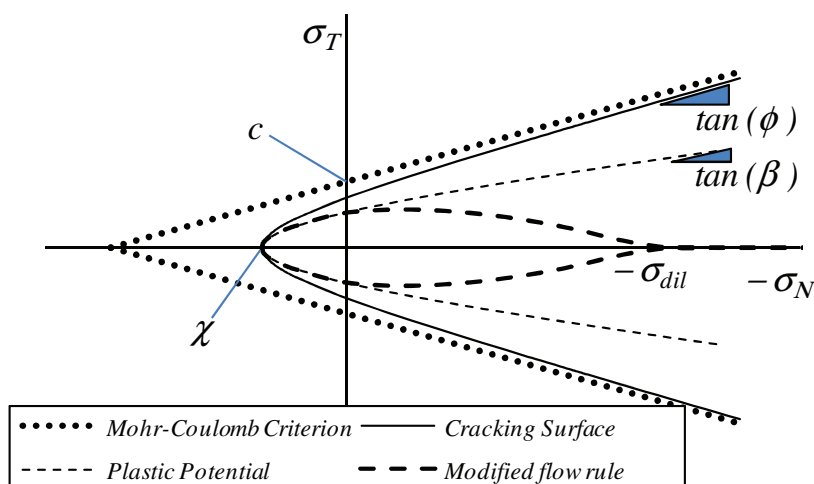
Figure 11: Failure hyperbola by Carol, Prat, & Lopez (1997), Mohr-Coulomb surface, plastic potential and modified flow rule.

The tensile strength χ (vertex of the hyperbola), the cohesion c and the frictional angle ϕ are material parameters needed for identifying the interface model. Eq. (7) outlines two principal failure modes:

- *Mode I type of fracture*: maximum strength surface is approached along its horizontal axis;

- *asymptotic Mode II type of fracture*: maximum strength surface is approached along its asymptotic zone, where the hyperbola approximates a Mohr-Coulomb criterion (see Figure 11).

Eq. (5) describes a general non-associated flow rule which controls the direction $\mathbf{m}$ of interface fracture displacements. In the proposed formulation the non-associated plastic direction is described by means of the transformation matrix operator $\mathbf{A}$

$$\mathbf{m} = \mathbf{A} \cdot \mathbf{n} \tag{8}$$

being

$$\mathbf{n} = \frac{\partial f}{\partial \mathbf{t}} = \left[\frac{\partial f}{\partial \sigma_\mathbf{N}}, \frac{\partial f}{\partial \sigma_\mathbf{T}}\right]^{\mathbf{t}} \tag{9}$$

the associated flow vector.

For the sake of brevity the description of the complete non-associated flow formulation is herein omitted. However further details can be founded in Caggiano et al. (2012).

In this formulation, the following unified function has been considered to model the softening of all internal parameters (controlling the interface yield criterion) under fracture processes and to incorporate self-healing effects during the time in Eq. (7)

$$p_i = (1 - (1 - r_{pi}) S[\xi_{p_i}]) SH[\psi] p_{0i} \tag{10}$$

where p_i alternatively equals χ, c or $tan\phi$, being $p_i = p_{0i}$ their initial values and r_{pi} the residual parameters.

The proposed scaling function $S[\xi_{p_i}]$ is

$$S[\xi_{p_i}] = \frac{e^{-\alpha_{p_i}\xi_{p_i}}}{1 + (e^{-\alpha_{p_i}} - 1)\xi_{p_i}} \tag{11}$$

whereby parameter α_{p_i} controls the decay form of the internal parameter as shown in Figure 12, while the non-dimensional variable ξ_{p_i} introduces the influence of the ratio between the current fracture work spent and the available fracture energies (G_f^I and G_f^{IIa})

$$\xi_\chi = \begin{cases} \frac{1}{2}\left[1 - cos\left(\frac{\pi w_{cr}}{G_f^I}\right)\right] & \text{if } w_{cr} \leq G_f^I \\ 1 & \text{otherwise} \end{cases} \tag{12}$$

$$\xi_c = \xi_{\tan\phi} = \begin{cases} \frac{1}{2}\left[1 - cos\left(\frac{\pi w_{cr}}{G_f^{IIa}}\right)\right] & \text{if } w_{cr} \leq G_f^{IIa} \\ 1 & \text{otherwise} \end{cases} \tag{13}$$

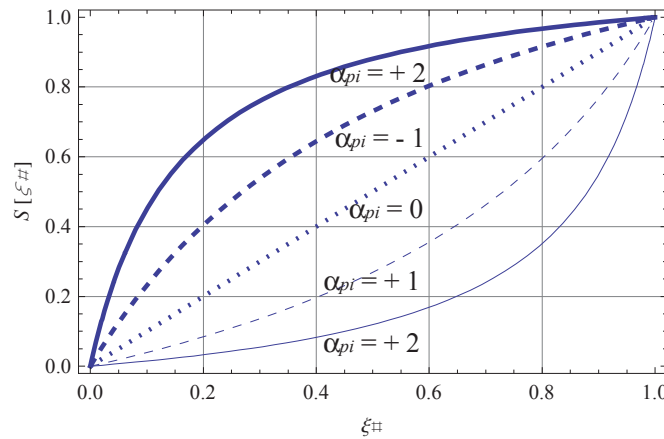according to the C^1 continuity function proposed by Caballero et al. (2008).

Figure 12: Scaling function $S[\xi_{p_i}]$ considering different values of α_{p_i}.

The fracture work spent w_{cr} during the opening-sliding fracture process controls the actual evolutions of the material parameters χ, c and $\tan\phi$ in softening regime of the interface constitutive law. The variable w_{cr}, defining the necessary amount of released energy to open a single crack in tensile and/or shear fracture mode due to normal σ_N and/or tangential σ_T joint stresses, has been reported in Caggiano et al. (2012).

$SH[\psi]$ in Eq. (10) is the proposed porosity-based rule for the self-healing description expressed as

$$SH[\psi] = 1 + (1 - P_{p_i}[\psi])sh \tag{14}$$

where sh (greater or equal than 0) is the self-healing scalar factor and

$$P_{p_i}[\psi] = \frac{e^{-\theta_{p_i}\psi}}{1 + (e^{-\theta_{p_i}} - 1)\psi} \tag{15}$$
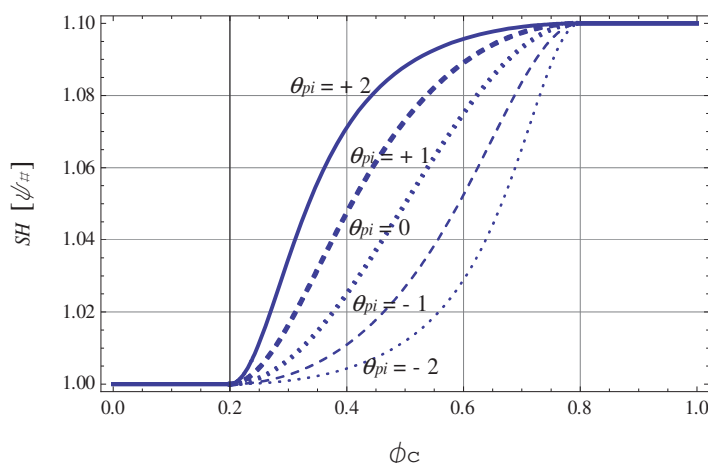
Figure 13: Porosity-based rule for the self-healing description $SH[\psi_\#]$ (with $\# = p_i$) vs. ϕ_c: as example $\phi_0 = 0.8$ and $\phi_f = 0.2$.

where the parameter ς_{p_i} defines several possible shapes of the porosity description as highlighted in Figure 13), while the ψ_{p_i} variable highlights the influence of the porosity through the following expression

$$\psi = \frac{1 - \cos\left(\pi \frac{\phi_c - \phi_0}{\phi_f - \phi_0}\right)}{2} \tag{16}$$

being ϕ_c the effective porosity (Lian et al., 2011) in the interface plane, while ϕ_0 and ϕ_f are two input parameters to be calibrated. Particularly, ϕ_0 represents the maximum reachable value of the effective porosity in the concrete matrix: e.g., concrete ideally without voids has $\phi_0 = 1$; ϕ_f represents that value of effective porosity at which the interface is totally softened: e.g. concrete ideally with 100% of voids deals with $\phi_f = 0$.

4 COMPARISON BETWEEN EXPERIMENTAL DATA AND NUMERICAL SIMULATIONS

This section proposes a preliminary calibration of the proposed interface model. For the calibration purpose, the experimental results on concrete specimens tested under three-point bending and presented in Section 2 are considered.

Figure 14 shows the 2-D geometry of the considered structure while Figure 15 highlights the FE discretization employed in the present analysis. Particularly, 4-node iso-parametric elements, equipped with a linear elastic model, have been adopted in the FE mesh. Then, all non-linearities are concentrated within zero-thickness interface elements defined throughout the adjacent edges of the finite elements in the central zone of the beam. Non-linear porosity and fracture-based laws were introduced in those interface elements according to the formulation outlined in Section 3.

The simulation of $100 \times 50 \times 450\ mm^3$ concrete specimens, tested under three-point bending according to Ferrara et al. (2014), is performed. Plane stress hypothesis and displacement-based control are assumed. For the purpose of the numerical evaluations, two material models were considered: (i) linear elastic material for concrete (describing the continuous elements) and (ii) elasto-plastic interface model (for interface elements). The key geometric and material properties were chosen according to the experimental evidences by Ferrara et al. (2014). Based on the calibration procedure, the elastic modulus and Poisson's ratio of concrete was $E_c =$
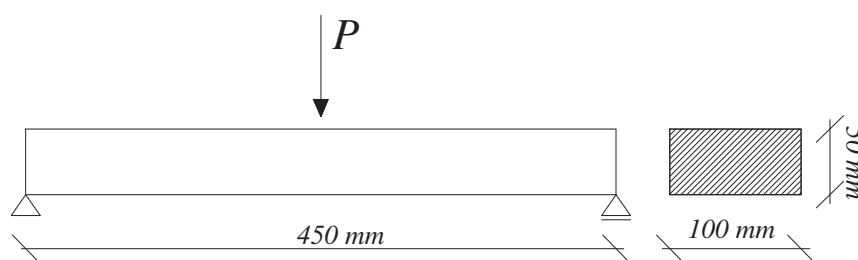
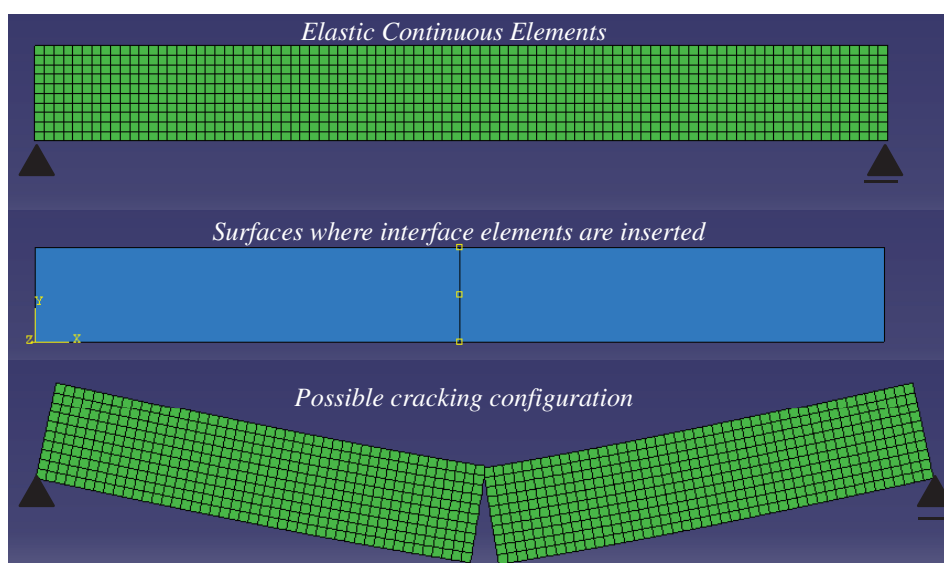Figure 14: Specimen geometry according to Ferrara et al. (2014) test.

Figure 15: Finite element mesh, interfaces and possible crack path of the three-point bending.

$21.7\,GPa$ and $\nu = 0.17$, respectively. Then, the mechanical parameters of the interface model are listed as follows: $k_N = 500\,MPa/mm$, $k_T = 200\,MPa/mm$, $\tan\phi_0 = 0.6$, $\tan\beta = 0.3$, $r_{tan\phi} = 0.67$, $\chi_0 = 2.5\,MPa$, $c_0 = 5.0\,MPa$, $G_f^I = 0.065\,N/mm$, $G_f^{IIa} = 0.650\,N/mm$, $\sigma_{dil} = 10\,MPa$, $\alpha_\chi = 0.5$, $\phi_c = 0.46$, $\phi_0 = 0.80$, $\phi_f = 0.20$, $sh = 0.3$ and all remaining parameters were considered null.

As example, Figure 16 shows the force-deflection curves against corresponding experimental results. It can be observed that the post-cracking response is well captured through the considered discontinuous approach based on non-linear interfaces. Furthermore, the comparison between the experimental and numerical results in terms of the load vs. COD highlights as the model is able to predict the self-healing recovery of the load bearing capacity with respect to the unloading value at which the value decayed in the pre-cracking stage. A recovery of the flexural load equals to about $250N$ is well reproduced by the numerical model, which corresponds to a recovery of about 17% of the maximum load capacity. However, and due to re-hydration self-healing phenomenon, a significant increase of the fracture energy takes place in the second-stage (post-treatment) of results of the analyzed three-point bending tests. This aspect is weakly predicted by the present model, further extension and enhancement of the proposed methodology will be addressed in future developments of the current research.

5 CONCLUDING REMARKS

This paper addressed the self-healing capacity of cementitious composites through both experiments and modeling. The experimental methodology outlined in this paper allows to pro-
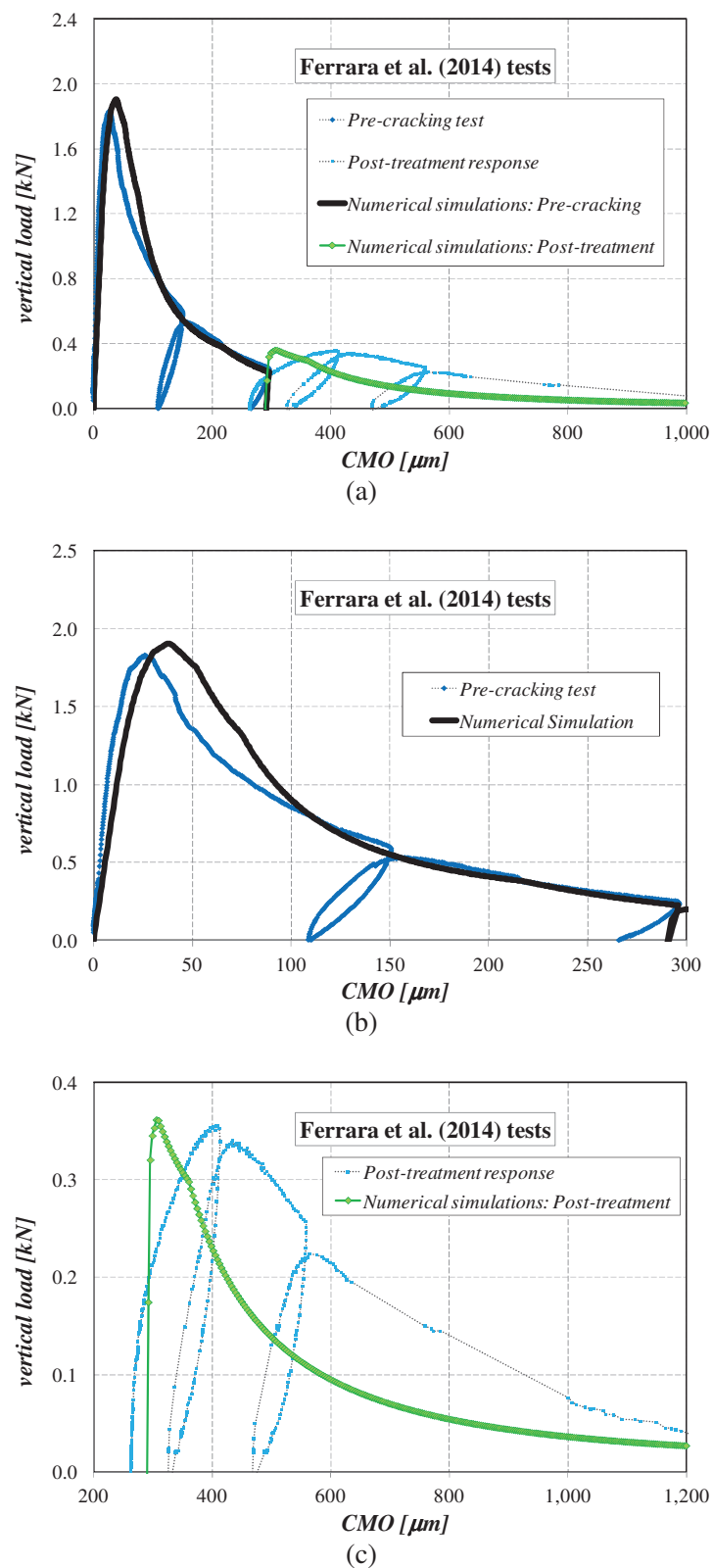
Figure 16: Load-deflection behavior on three-point beam: experimental results (Ferrara et al., 2014) vs. numerical predictions.

vide quantification of crack closure due to self-healing in concrete. Based on those preliminary results, the self-healing efficiency in concrete increases with the presence crystalline additive.

Immersion in water leads to higher self-healing capacity, especially observed in higher crack widths. Moreover, the formulation of a novel porosity and fracture-based model for concrete interfaces was proposed. The proposal reported a quadratic hyperbola as a maximum strength criterion of the interface, defining the interaction between maximum shear and normal interface stresses. Such a formulation explicitly considered the porosity evolutions due to self-healing pore closures accounted into the failure surface and the post-cracking response through a function which modifies the strength parameters and the softening law. Numerical analyses, performed with the constitutive model presented in this paper, demonstrate its predictive capabilities in terms of the most relevant aspects of the mechanical behavior of concrete after crack closure due to self-healing. Further developments are currently ongoing in order to improve the proposed model. The assessment and identification of the present model to simulate the behavior of concrete members under more complex loading and self-healing phenomena, including mesoscopic analysis with the employment of the proposed interface model, is another objective of future researches.

ACKNOWLEDGMENT

REFERENCES

Caballero A., Willam K., and Carol I. Consistent tangent formulation for 3D interface modeling of cracking/fracture in quasi-brittle materials. *Computer Methods in Applied Mechanics and Engrg.*, 197:2804–2822, 2008.

Caggiano A., Etse G., and Martinelli E. Zero-thickness interface model formulation for failure behavior of fiber-reinforced cementitious composites. *Computers & Structures*, 98-99(0):23 – 32, 2012.

Carol I., Prat P., and Lopez C. Normal/shear cracking model: Applications to discrete crack analysis. *J. of Engrg. Mechanics - ASCE*, 123:765–773, 1997.

Di Luzio G. and Cusatis G. Solidification-microprestress-microplane (SMM) theory for concrete at early age: Theory, validation and application. *International Journal of Solids and Structures*, 50(6):957–975, 2013.

Di Luzio G., Ferrara L., and Krelani V. A numerical model for the self-healing capacity of cementitious composites. In *Proceedings of EURO-C 2014, Pages 741-747*, volume 2. 2014.

Edvardsen C. Water permeability and autogenous healing of cracks in concrete. *ACI Materials Journal*, 96(4), 1999.

Ferrara L., Krelani V., and Carsana M. A fracture testing based approach to assess crack healing of concrete with and without crystalline admixtures. *Construction and Building Materials - In Press*, 2014.

Granger S., Loukili A., Pijaudier-Cabot G., and Chanvillard G. Experimental characterization of the self-healing of cracks in an ultra high performance cementitious material: Mechanical tests and acoustic emission analysis. *Cement and Concrete Research*, 37(4):519 – 527, 2007.

He H., Guo Z., Stroeven P., and Stroeven M. Numerical assessment of concrete's self-healing potential for promoting durability. *International Journal of Modelling, Identification and*

Control, 7(2):142–147, 2009.

He H., Guo Z., Stroeven P., Stroeven M., and Sluys L.J. Self-healing capacity of concrete-computer simulation study of unhydrated cement structure. *Image Analysis & Stereology*, 26(3):137–143, 2011.

Hearn N. and Morley C. Self-sealing property of concrete-experimental evidence. *Materials and structures*, 30(7):404–411, 1997.

Hilloulin B., Grondin F., Matallah M., and Loukili A. Modelling of autogenous healing in ultra high performance concrete. *Cement and Concrete Research*, 61-62(0):64 – 70, 2014.

Huang H. and Ye G. Simulation of self-healing by further hydration in cementitious materials. *Cement and Concrete Composites*, 34(4):460–467, 2012.

Lian C., Zhuge Y., and Beecham S. The relationship between porosity and strength for porous concrete. *Construction and Building Materials*, 25(11):4294 – 4298, 2011.

Mihashi H. and Nishiwaki T. Development of engineered self-healing and self-repairing concrete-state-of-the-art report. *Journal of Advanced Concrete Technology*, 10(5):170–184, 2012.

Neville A. Autogenous healing: A concrete miracle? *Concrete International*, 24(11), 2002.

new Model-Code. *Model Code 2010 - First complete draft, Vol. 1.* Comite Euro-International du Beton-Federation International de la Precontrainte, Paris, 2010.

Reinhardt H.W. and Jooss M. Permeability and self-healing of cracked concrete as a function of temperature and crack width. *Cement and Concrete Research*, 33(7):981–985, 2003.

Sisomphon K., Copuroglu O., and Koenders E. Self-healing of surface cracks in mortars with expansive additive and crystalline additive. *Cement and Concrete Composites*, 34(4):566–574, 2012.

Van Tittelboom K. and De Belie N. Self-healing in cementitious materials-a review. *Materials*, 6(6):2182–2217, 2013.

Wu M., Johannesson B., and Geiker M. A review: Self-healing in cementitious materials and engineered cementitious composite as a self-healing material. *Construction and Building Materials*, 28(1):571–583, 2012.

Yang Y., Lepech M.D., Yang E.H., and Li V.C. Autogenous healing of engineered cementitious composites under wet–dry cycles. *Cement and Concrete Research*, 39(5):382–390, 2009.